Korea-Australia Rheology Journal
Vol. 21, No. 1, March 2009 pp. 27-37

Effect of viscoelasticity on two-dimensional laminar vortex shedding in flow past a rotating cylinder

Ju Min Kim[1], Kyung Hyun Ahn[2,*] and Seung Jong Lee[2]
[1]*Department of Chemical Engineering, Ajou University, Suwon 443-749, Korea*
[2]*School of Chemical and Biological Engineering, Seoul National University, Seoul 151-744, Korea*
(Received October 18, 2008; final revision received November 29, 2008)

Abstract

In this work, we numerically investigate the effect of viscoelasticity on 2D laminar vortex dynamics in flows past a single rotating cylinder for rotational rates $0 \leq \alpha \leq 5$ (the rotational rate α is defined by the ratio of the circumferential rotating velocity to free stream velocity) at Re=100, in which the vortex shedding has been predicted to occur in literature for Newtonian fluids. The objective of the present research is to develop a promising technique to fully suppress the vortex shedding past a bluff body by rotating a cylinder and controlling fluid elasticity. The predicted vortex dynamics with the present method is consistent with the previous works for Newtonian flows past a rotating cylinder. We also verified our method by comparing our data with the literature in the case of viscoelastic flow past a non-rotating cylinder. For $0 \leq \alpha \leq 1.8$, the frequency of vortex shedding slightly decreases but the fluctuation of drag and lift coefficient significantly decreases with increasing fluid elasticity. We observe that the vortex shedding of viscoelastic flow disappears at lower α than the Newtonian case. At $\alpha=5$, the relationship between the frequency of vortex shedding and Weissenberg number (Wi) is predicted to be non-monotonic and have a minimum around Wi=0.25. The vortex shedding finally disappears over critical Wi number. The present results suggest that the vortex shedding in the flow around a rotating cylinder can be more effectively suppressed for viscoelastic fluids than Newtonian fluids.

Keywords : viscoelastic fluid flow; vortex shedding, rotating cylinder

1. Introduction

The flow instabilities of viscoelastic fluids have been observed in some creeping flows, *e.g.*, unsteady flows over critical Weissenberg number in a contraction geometry (Rothstein and McKinley, 1999; Nigen and Walters, 2002), wake instability around a confined cylinder (McKinley *et al.*, 1993), 'fibril-formation' instability in a filament stretching rheometer (Spiegelberg and McKinley, 1996) and elastic turbulence (Groisman and Steinberg, 2000). Many researchers have attempted to analyze the physics behind these phenomena (McKinley *et al.*, 1996; Graham, 2003). From the aspect of numerical scheme, several transient FEM (Finite Element Method)-based or FVM (Finite Volume Method)-based schemes have been proposed to capture the fully transient viscoelastic flow phenomena: θ-method (Saramito and Piau, 1994), Runge-Kutta 4th order formulation (Caola *et al.*, 2001), TG (Taylor-Galerkin) (Carew *et al.*, 1993), and SIMPLE-series algorithm for FVM (Alves *et al.*, 2001). However, it is still challenging to numerically predict the instabilities of viscoelastic flows. Transient schemes have also merit such that huge coupled equations can be divided into small sub-problems at each time step. Thus, these methods can also be applied to obtain steady solutions (Carew *et al.*, 1993; Caola *et al.*, 2001; Alves *et al.*, 2001).

Viscoelasticity can affect vortex dynamics in high Reynolds number flows, *e.g.*, turbulent drag reduction has been extensively studied (Sureshkumar *et al.*, 1997; Dimitropoulos *et al.*, 1998; Min *et al.*, 2001; Min *et al.*, 2003). Viscoelasticity can also play an important role in laminar vortex shedding (Oliveira, 2001; Sahin and Owens, 2004; Oliveira and Miranda, 2005) which is generated at lower Reynolds number than turbulent flow. The wake instabilities behind a stationary/rotating cylinder are still active research areas even for Newtonian fluid. Flow past a stationary cylinder has been considered to be a benchmark problem in conventional computational fluid dynamics and the diverse vortex modes can be generated in stationary cylinder problems as a function of Reynolds number (Re). The detailed discussion and review can be found in Williamson (1996): the flow remains steady under Re=47, becomes unsteady over Re=47 and shows three-dimen-

*Corresponding author: ahnnet@snu.ac.kr

sional and chaotic turbulence over Re=200. Re is defined by $du_\infty\rho/\eta_0$, where d is the diameter of cylinder, u_∞ is the free-stream velocity, ρ the fluid density, and η_0 the fluid viscosity. The flow past a constantly rotating cylinder has been investigated for Newtonian fluids (Kang *et al.*, 1999; Stojković *et al.*, 2002; Stojković *et al.*, 2003; Kang, 2006). Kang *et al.* (1999) employed fully implicit fractional step method with finite difference method and showed that the vortex shedding disappears in the range of the rotational rate α larger than the critical rotating rate α_L, where the rotational rate α is defined by the ratio of the circumferential rotating velocity to free-stream velocity u_∞ ($\alpha\equiv\Omega d/2u_\infty$), where Ω denotes the angular velocity of the cylinder. The critical rotational rate α_L is dependent upon Reynolds number (Re): α_L ranges from 0 to 2 for $40\leq$ Re$\leq$140 (Kang *et al.*, 1999). Thereby, they suggested that rotating the cylinder could be used to suppress vortex shedding to reduce the structural vibration, acoustic noise and resonance. Later, new secondary vortex shedding mode (Stojković *et al.*, 2003) was found at higher rotating rates than the conditions of Kang *et al.* (1999). Stojković *et al.* (2003) showed that there exist wake instabilities with longer wavelengths compared with the traditional von Kármán vortex. The vortex mode was predicted at high α values within narrow region (Stojković *et al.*, 2003). Stojković *et al.* (2003) showed four different vortex modes according to α: vortex shedding exists at low value of $0\leq\alpha\leq\alpha_{L(I)}$, vortex shedding is suppressed in the moderate range of $\alpha_{L(I)}<\alpha\leq\alpha_{L(II)}$, the new secondary vortex shedding is generated at higher values of $\alpha_{L(II)}<\alpha\leq\alpha_{L(III)}$, and the vortex shedding is suppressed for $\alpha>\alpha_{L(III)}$. For instance, Stojković *et al.* (2003) showed that $\alpha_{L(I)}$ is predicted to be 1.8, $\alpha_{L(II)}$=4.8, and $\alpha_{L(III)}$=5.15 at Re=100, respectively. They also showed that $\alpha_{L(I)}$ increases with increasing Re, while $\alpha_{L(II)}$ and $\alpha_{L(III)}$ decrease. The Strouhal number (St) of the secondary vortex shedding decreases with increasing α at fixed Re, where St is defined by $1/T$ and T corresponds to the period of the vortex shedding.

In computational rheology, there have been several researches to investigate the effect of viscoelasticity on vortex shedding in flows past a cylinder (Oliveira, 2001; Sahin and Owens, 2004; Oliveira and Miranda, 2005). Oliveira (2001) employed FVM to investigate the viscoelastic effect on vortex shedding in unbounded domains. Oliveira (2001) showed that elasticity reduces St and suppresses the fluctuation of drag and lift magnitude, which is consistent with experimental results (Usui *et al.*, 1980; Cadot and Lebey, 1999; Cadot and Kumar, 2000). Sahin and Owens (2004) performed linear stability analysis. They employed 'velocity-only' FVM to explore the influence of elasticity on the vortex shedding in flow past a confined cylinder. They showed that the amplitude and frequency of vortex shedding in viscoelastic flows are lower than for Newtonian case (Sahin and Owens, 2004), of which the qualitative trend is consistent with those in unbounded domain predicted by Oliveira (2001).

Two strategies have previously been used to stabilize vortex shedding around a cylinder: rotating cylinder and controlling the fluid viscoelasticity. Thus, we assume that rotating cylinder coupled with viscoelastic flow may produce more synergetic effect on suppressing vortex shedding. In the present work, we will verify this assumption by investigating how viscoelasticity affects the characteristics of flows around a rotating cylinder in unbounded flow. In this work, we will focus on the influence of viscoelasticity on the secondary vortex shedding mode as was found by Stojković *et al.* (2003), according to which the vortex shedding is eventually suppressed at high rotational rates ($\alpha>\alpha_{L(III)}$) for Newtonian fluids. This paper will show that the vortex shedding can be suppressed for viscoelastic fluid flows at lower rotational rate ($\alpha<\alpha_{L(III)}$). The present work will be helpful for future experimental design and will provide a useful strategy to suppress the vortex shedding which is unavoidable in flows around stationary bluff bodies at high Reynolds number.

This paper is organized as follows. In the following sections, the governing equations and numerical schemes are presented. In Sec. 4, we verify the reliability of the present numerical scheme as well as the numerical parameters adopted in the present study. Next, we will successively discuss the effects of viscoelasticity on vortex dynamics for rotational rates $0\leq\alpha\leq2$, and at $\alpha=5$.

2. Governing equations

In this work, the transient problem is considered with inertia. We employ the inertial momentum equation and incompressibility constraint. The modified FENE-CR model is used as a constitutive equation, which was also used to investigate the viscoelastic effect on vortex shedding around a stationary cylinder previously (Oliveira, 2001). The dimensionless momentum equation, incompressibility constraint and the constitutive equation can be denoted as follows:

$$Re\left(\frac{\partial \boldsymbol{u}}{\partial t}+\boldsymbol{u}\cdot\nabla\boldsymbol{u}\right)=-\nabla p+\beta\nabla\cdot(\nabla\boldsymbol{u}+(\nabla\boldsymbol{u})^T)+\nabla\cdot\tau_p, \tag{1}$$

$$\nabla\cdot\boldsymbol{u}=0, \tag{2}$$

$$\tau_p+\frac{Wi}{f(\tau_p)}\tau_{p(1)}=(1-\beta)(\nabla\boldsymbol{u}+(\nabla\boldsymbol{u})^T),$$

$$f(\tau_p)=\frac{L^2+(Wi/(1-\beta))tr(\tau_p)}{L^2-3}, \tag{3}$$

where $\boldsymbol{u}$ is non-dimensionalized velocity with a characteristic velocity u_∞, τ_p and p are non-dimensionalized extra stress and pressure with η_0u_∞/H, respectively. The Weissenberg number Wi is defined by $\lambda u_\infty/d$, where λ is the

relaxation time of polymer solution. The retardation ratio $\beta \equiv \eta_s/\eta_0$ is the ratio of solvent viscosity (η_s) and solution viscosity (η_0), and is taken to be ($\beta \equiv \eta_s/\eta_0 = 1.0/1.1$) in accordance with Oliveira (2001). In Eq. (3), the extensibility parameter L^2 is set to 100 following Oliveira (2001). $\tau_{p(1)}$ is the upper-convected derivative of tensor t_p defined as follows:

$$\tau_{p(1)} = \frac{\partial \tau_p}{\partial t} + \boldsymbol{u}\cdot\nabla\tau_p - (\nabla \boldsymbol{u})^T\cdot\tau_p - \tau_p\cdot(\nabla \boldsymbol{u}) \tag{4}$$

We set Re to be 100 throughout this work. The laminar vortex shedding regime ranges from Re=47 to Re=200 and the flows at Re=100 have been explored by many previous researches (Kang *et al.*, 1999; Oliveira, 2001; Stojković *et al.*, 2003) and thus, direct comparison between ours and the literature is possible.

3. Numerical method

3.1. Finite element formulation, transient scheme and stabilization techniques

The computational domain Ω is discretized into quadrilateral finite elements R_e so that $\Omega = \cup R_e$ and $\phi = \cap R_e$. In this study, the velocity, pressure and extra stress are approximated in terms of Lagrangian basis functions as follows:

$$\boldsymbol{u} = \sum_i \Psi_i u_i,\ p = \sum_i \phi_i p_i.$$

$$\boldsymbol{S} = \sum_i \phi_i S_i, \tag{5}$$

where $\boldsymbol{S}$ denotes τ_p and ϕ_i and ψ_i are the bilinear and biquadratic basis functions, respectively.

In the present work, the following fully implicit BDF2 (the 2-step backward difference formula) scheme is adopted for time forwarding:

$$\frac{\partial(\ )}{\partial t} = \frac{3(\ )^{n+1} - 4(\ )^n + (\ )^{n-1}}{2\Delta t}. \tag{6}$$

where ( ) corresponds to a variable in the transient equation, *e.g.*, $\boldsymbol{u}$ in Eq. (1). BDF2 has 2nd order accuracy and A-stable (Deville *et al.*, 2002), and this formulation was previously applied to the finite volume method by Oliveira (2001). Oliveira (2001) showed that BDF2 was superior to 1st order Euler scheme in the aspect of accuracy.

The final weak forms of Eqs. (1)-(3) are;

$$\left\langle Re\left(\frac{3\boldsymbol{u}^{n+1} - 4\boldsymbol{u}^n + \boldsymbol{u}^{n-1}}{\Delta t} + \boldsymbol{u}^{n+1}\cdot\nabla\boldsymbol{u}^{n+1}\right); \psi\right\rangle$$

$$+\left\langle -p^{n+1}\boldsymbol{I} + \beta(\nabla\boldsymbol{u}^{n+1} + (\nabla\boldsymbol{u}^{n+1})^T) + \boldsymbol{S}^{n+1}; \nabla\psi\right\rangle$$

$$= \left\langle \left\langle (-p^{n+1}\boldsymbol{I} + \beta(\nabla\boldsymbol{u}^{n+1} + (\nabla\boldsymbol{u}^{n+1})^T) + \boldsymbol{S}^{n+1})\cdot\boldsymbol{n}; \psi\right\rangle\right\rangle, \tag{7}$$

$$\langle \nabla\cdot\boldsymbol{u}^{n+1}; \phi\rangle = 0, \tag{8}$$

$$\left\langle \boldsymbol{S}^{n+1} + \frac{Wi}{f}\left(\frac{3\boldsymbol{S}^{n+1} - 4\boldsymbol{S}^n + \boldsymbol{S}^{n-1}}{\Delta t} + \boldsymbol{u}^{n+1}\cdot\nabla\boldsymbol{S}^{n+1}\right.\right.$$

$$\left.\left. - (\nabla\boldsymbol{u}^{n+1})^T\cdot\boldsymbol{S}^{n+1} - \boldsymbol{S}^{n+1}\cdot\nabla\boldsymbol{u}^{n+1}\right); \phi\right\rangle$$

$$= \langle (1-\beta)(\nabla\boldsymbol{u}^{n+1} + (\nabla\boldsymbol{u}^{n+1})^T); \phi\rangle$$

$$f(\boldsymbol{S}^{n+1}) = \frac{L^2 + (Wi/(1-\beta))tr(\boldsymbol{S}^{n+1})}{L^2 - 3}, \tag{9}$$

where $\boldsymbol{I}$ is the unit tensor and $\boldsymbol{n}$ denotes outward normal vector at the boundary. The symbols <;> and <<;>> stand for domain and boundary integral, respectively. In this work, the streamline upwind/Petrov-Galerkin (SU/PG) method (Brooks and Hughes, 1982) is adopted as a stabilization technique and consistently applied to the constitutive equation. We employed the modified SU/PG version by Fan and Crochet (1995). In the SU/PG method, the weight function is modified as follows:

$$\phi_m = \phi + \bar{k}w\cdot\nabla\phi \tag{10}$$

where ϕ_m is the modified weight function and ϕ is the regular weight function as in Eq. (5). $\bar{k}$ is defined as a characteristic length of finite element and $w = \frac{\boldsymbol{u}}{|\boldsymbol{u}|_a}$ and $|\boldsymbol{u}|_a = \frac{1}{4}\sum_i |u_i|$, where $|u_i|$ is the magnitude of velocity at the vertices of the element (Fan and Crochet, 1995). Finally, it is to be noted that we do not employ DEVSS-G (discrete elastic viscous split stress) formulation which is also one of the standard stabilization techniques because the additional variable (velocity gradient tensor) in DEVSS-G formulation increases the computational cost and the stable computation in the present work can be attributed to the small polymer contribution to the solution viscosity ($\eta_p/\eta_0 = 0.1/1.1$), where η_p is polymer viscosity.

3.2. Solution method

At each time step, fully coupled non-linear equations of $\boldsymbol{u}$, p and $\boldsymbol{S}$ are solved. Newton-Raphson method is employed to linearize the nonlinear equations (7)-(9) as follows: $(\boldsymbol{u},p,\boldsymbol{S})^{i+1} = \Delta(\boldsymbol{u},p,\boldsymbol{S}) + (\boldsymbol{u},p,\boldsymbol{S})^i$ where i denotes the number of iteration step. The linearized equations are solved with the previously developed iterative scheme (Kim *et al.*, 2004) except that there is no velocity gradient tensor in the present work. Thus, two convergence criteria are necessary. One criterion for the Newton-Raphson outer loop is set to the L_1 norm of $\Delta(\boldsymbol{u},p,\boldsymbol{S}) < 10^{-4}$. The convergence criterion for the iterative solver (BiCGSTAB solver (van der Vorst, 1992)) is set to L_2 norm $< 10^{-6}$.

4. Results and discussion

4.1. Problem description, boundary conditions and finite elements

In this work, we focus on the viscoelastic effect on the vortex shedding past a rotating cylinder in unbounded domain. As shown in Fig. 1, the computational domain is

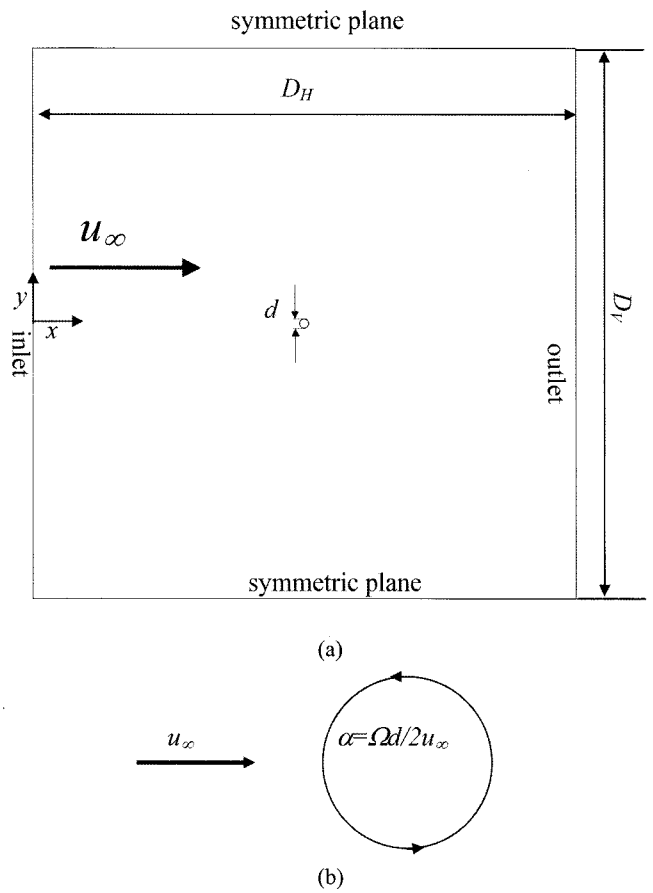

Fig. 1. Schematic diagram of vortex shedding in the flow past a rotating cylinder in an unbounded domain: (a) the whole domain, (b) magnified view near a cylinder. Note that the length scale is non-dimensionalized with the cylinder diameter d. In Fig. 1 (b), u_∞ denotes the free stream velocity and α corresponds to the ratio of rotational velocity at the cylinder wall to the free stream velocity, where Ω is the constant angular velocity of the rotating cylinder. The cylinder is rotating in counter clockwise direction.

a square containing a cylinder with the diameter d at the center. To accurately resolve the problem, it is expected that the larger computational domain size yields the better numerical solutions for the unbounded flows. However, there should be a trade-off between accuracy and computational resources. In this work, the size of the computational domain is denoted by $D_H \times D_V$, where D_H and D_V are the domain lengths in the stream and cross-stream directions, respectively and we chose $D_H=D_V$. Oliveira (2001) compared two computational domain sizes to consider the unbounded flow around a stationary cylinder: $60d\times60d$ ($D_H\times D_V$) and $45d\times30d$ ($D_H\times D_V$). They concluded that $45d\times30d$ ($D_H\times D_V$) is sufficient to simulate vortex shedding around the stationary cylinder problem. Thus, the domain size larger than $45d\times30d$ ($D_H\times D_V$) is sufficient to mimic the unbounded flows. The rotational flow around a rotating cylinder is involved in this work and

Table 1. Description of finite elements used in the present work

Mesh	Number of elements	Total number of nodes	Number of vertices	Total DOF
Mesh I	6,400	25,856	6528	77,824
Mesh II	14,400	57,920	14,560	174,080

thus, we chose a little larger $60d\times60d$ ($D_H\times D_V$) than that of Oliveira.

The uniform velocity boundary condition ($u=u_\infty$, $v=0$) is imposed on the inlet and the constant circumferential velocity ($\Omega d/2$) is prescribed on the cylinder wall. Symmetric boundary conditions are imposed on the upper and lower boundaries, and zero extra stresses are imposed on the inlet. Open boundary condition (OBC) or so-called 'no boundary condition' (Papanastasiou *et al.*, 1992) is imposed on outlet. In vortex shedding flow, as the flow field at outlet may change at each time step, the essential boundary condition or zero gradient velocity field boundary condition is not exact. Papanastasiou *et al.* (1992) employed OBC based on FEM and applied it to backward-step flow simulation with shorter flow geometry than expected to be fully developed flow field. OBC was successfully applied to non-isothermal viscoelastic flow simulation in axisymmetric 4:1 contraction flow simulation (Park and Lee, 1999) and co-extrusion flow simulation of viscoelastic flows (Sunwoo *et al.*, 2001).

In the present work, two different finite element meshes were considered and more refined Mesh II is used except mesh refinement test. We set the time increment Δt to be 0.05 or 0.025. In the following section, we will show that the selected numerical parameters are appropriate for the present problem. The detailed mesh information is pre-

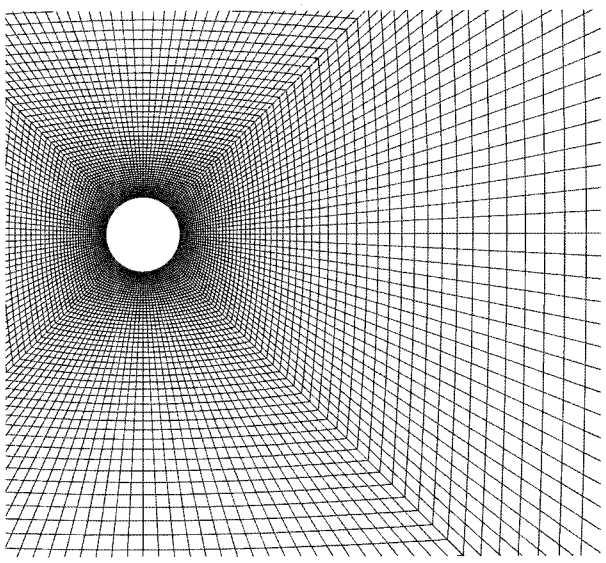

Fig. 2. Magnified view of Mesh II near the cylinder. The detailed mesh information is presented in Table 1.

Table 2. Comparison of physical data between the present work and literatures for Newtonian fluids

Quantities	Park *et al.* (1998), $\alpha=0.0$	Oliveira (2001) $\alpha=0.0$ (Mesh-3)	Lilek *et al.* (1997) $\alpha=0.0$	Stojković *et al.* (2002) $\alpha=0.0$	Mesh II $\alpha=0.0$ $\Delta t=0.05$	Kang *et al.* (1999) $\alpha=1.0$	Stojković *et al.* (2002) $\alpha=1.0$	Kang (2006) $\alpha=1.0$	Mesh II $\alpha=1.0$ $\Delta t=0.05$
$C_{D(avg)}$	1.33	1.3701	1.3566	1.3371	1.3348	1.1040	1.1080	1.1120	1.1045
$C_{L(avg)}$	0	0	0	0	0	2.4881	2.5040	2.4787	2.5081
$C_{D(fluc)}$	0.0091	0.0099	0.0097	0.0091	0.0092	0.0993	0.0986	0.0997	0.0977
$C_{L(fluc)}$	0.3321	0.3425	0.3400	0.3259	0.3246	0.3631	0.3616	0.3675	0.3586
$St=fd/u_\infty$	-	0.1670	0.1699	0.1650	0.1653	0.1655	0.1658	0.1654	0.1653

sented in Table 1 and the magnified view of Mesh II is presented in Fig. 2.

4.2. Accuracy

We checked mesh-dependence and time increment-dependence in typical flow conditions and compared the obtained numerical solutions with previous results in literatures. First, we compared the present results with previous ones for Newtonian fluid, where all computations were performed with Mesh II. We set $\Delta t=0.05$ since this setting was used by Oliveira (2001) (note that Oliveira (2001) also used BDF2 as a time-marching scheme). Later, we will investigate the effect of Δt. The drag and lift coefficients are defined as $C_D = 2f_x/\rho u_\infty^2 d$ and $C_L = 1/2 f_y/\rho u_\infty^2 d$, respectively, where f_x and f_y are x- and y- components of the force exerting on the cylinder wall. The average drag and lift coefficients are defined with $C_{D(avg)} = 2(C_{D_{max}} + C_{D_{min}})$ and $C_{L(avg)} = 1/2(C_{L_{max}} + C_{L_{min}})$, respectively, where the subscripts 'max' and 'min' denote the maximum and minimum values in one period (we note that $C_{D(avg)}$ and $C_{L(avg)}$ are defined in steady oscillatory vortex shedding). The fluctuations of drag and lift coefficients are defined as $C_{D(fluc)} = 1/2(C_{D_{max}} - C_{D_{min}})$ and $C_{L(fluc)} = 1/2(C_{L_{max}} - C_{L_{min}})$, respectively. As shown in Table 2, the present results are consistent with previous results for both stationary ($\alpha=0$) and rotating cylinder cases ($\alpha=1$). Thus, the present numerical method and numerical parameters are appropriate for the present problem. For viscoelastic case (FENE-CR fluid), the comparison between ours and those of Oliveria (2001) is presented in Table 3. There is good agreement between two data sets at Wi=4 and $\alpha=0$. Thus, Mesh II is sufficiently refined for the present problem and all compu-

Table 3. Comparison of physical data between the present work and literature

Quantities	Oliveira (2001) $\Delta t=0.05$ $\alpha=0.0$, Wi=4	Mesh II $\alpha=0.0$, $\Delta t=0.05$, Wi=4	Mesh II $\alpha=0.0$, $\Delta t=0.025$, Wi=4
$C_{D(avg)}$	1.3296	1.2884	1.2886
$C_{L(avg)}$	0	0	0
$C_{D(fluc)}$	0.0035	0.0032	0.0033
$C_{Lfluc)}$	0.1977	0.1898	0.1902
$St=fd/u_\infty$	0.1597	0.1587	0.1584

Table 4. Mesh refinement test. We note that the computational times with Mesh I and Mesh II are 1606 and 4494 seconds for 100 time steps at $\alpha=1$, $\Delta t=0.025$ and Wi=0, respectively. The computational time was checked using Intel® Core™ 2 Duo CPU E4500 @2.2 GHZ with 2.0 GB RAM.

Quantities	Mesh I $\alpha=1$, $\Delta t=0.025$, Wi=0	Mesh II $\alpha=1$, $\Delta t=0.025$, Wi=0	Mesh I $\alpha=1$, $\Delta t=0.025$, Wi=2	Mesh II $\alpha=1$, $\Delta t=0.025$, Wi=2
$C_{D(avg)}$	1.1020	1.1046	1.0507	1.0468
$C_{L(avg)}$	−2.5057	−2.5081	−2.4623	−2.4626
$C_{D(fluc)}$	0.0977	0.0977	0.0683	0.0610
$C_{Lfluc)}$	0.3565	0.3587	0.2340	0.2153
$St=fd/u_\infty$	0.1660	0.1653	0.1633	0.1633

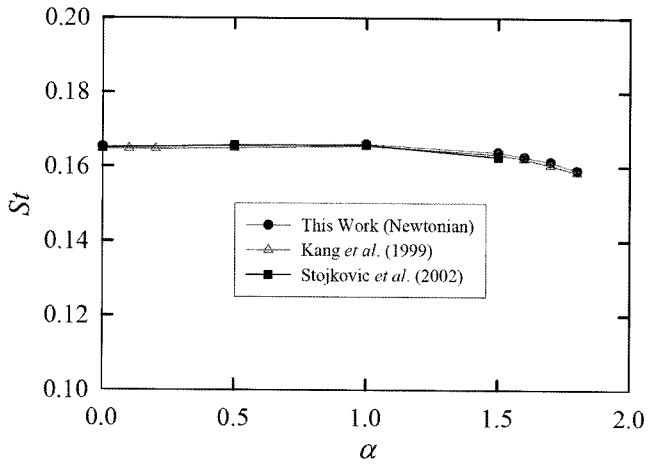

Fig. 3. Comparison of present results with previous data with a for the range of $0 \le \alpha \le 2.0$ at Re=100. We note that vortex shedding disappears for $\alpha > 1.8$.

tations are performed with Mesh II from now on (*cf.* mesh refinement test is presented in Table 4). As shown in Table 3, we also investigated the effect of time discretization and the difference between $\Delta t = 0.05$ and $\Delta t = 0.025$ was found to b e negligible. Thus, we conclude that the Δt below 0.05 is sufficient for the present problem.

4.3. Flow behaviors

Kang *et al.* (1999) performed numerical simulation with Newtonian fluid for $0 \le \alpha \le 2.5$ at several Reynolds numbers. They reported that vortex shedding completely disappears for $\alpha > 1.8$ at Re=100. Stojković *et al.* (2003) investigated the same problem with wider ranges of a than Kang *et al.*, *i.e.*, $0 < \alpha < 12$. Stojković *et al.* (2003) found that new secondary vortex mode appears within very small range of a at higher rotation rate, *e.g.*, $4.8 \le \alpha \le 5.15$ at Re=100. In the present work, we investigated the effect of elasticity on vortex shedding at Re=100 in two regimes

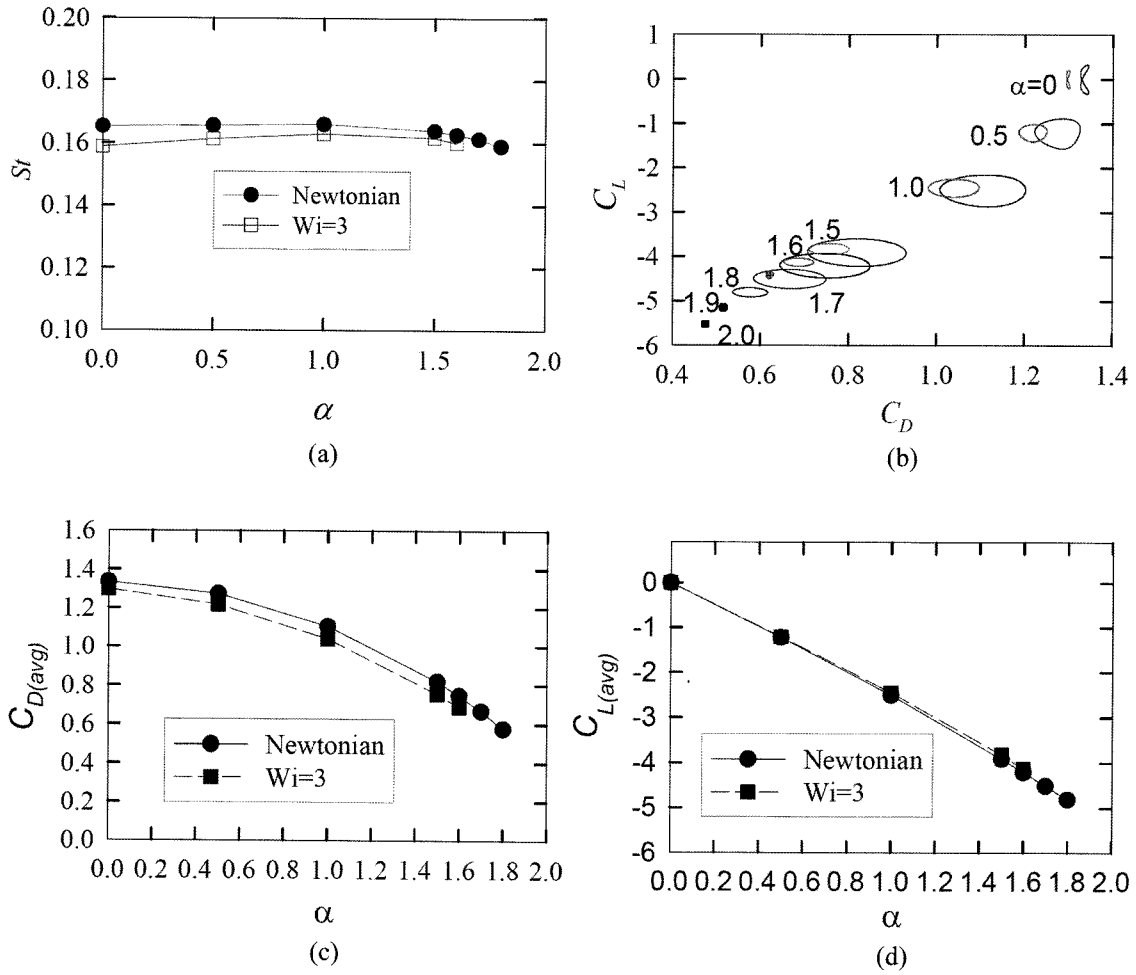

Fig. 4. Viscoelastic effect on the steady state vortex shedding: (a) St vs a, (b) C_L vs C_D, (c) average C_D , and (d) average C_L. Note that the vortex shedding occurs in the range of $0 \le \alpha \le 1.8$ for Newtonian fluid and the range was reduced to $0 \le \alpha \le 1.6$ for viscoelastic fluid at Wi=3. In Fig. 4(b), black and red lines correspond to Newtonian and viscoelastic fluid at Wi=3 cases, respectively. We successively show C_L-C_D trajectories corresponding to α=0, 0.5, 1.0, 1.5, 1.6, 1.7, 1.8, 1.9 and 2.0 (for Newtonian fluid) and α=0, 0.5, 1.0, 1.5, 1.6, 1.7 (for viscoelastic fluid at Wi=3) from right-up to left-bottom.

where vortex shedding exists; $0 \le \alpha \le 2$ and $\alpha = 5$, in which the latter was selected as a typical value in the regime where the secondary vortex mode is generated.

Variation of St vs. α is presented in Fig. 3 for Newtonian fluids in the range of $0 \le \alpha \le 2.0$ at Re=100. In the present work, vortex shedding completely disappears at $\alpha > 1.8$ for Newtonian fluid, which is consistent with previous works (Kang *et al.*, 1999; Stojković *et al.*, 2003; we note that the results of Kang (2006) which are not presented here are also consistent with those of Kang *et al.* (1999)). As shown in Fig. 3, St is nearly independent of α before the disappearance of vortex shedding. The independence of St upon α was observed by Kang *et al.* (1999) and Stojković *et al.* (2003) at various Reynolds numbers. The agreement between ours and the literatures in the relationship between St and α confirms that our numerical scheme and parameter settings are sufficiently accurate for the present problem. Next, we investigate the effect of viscoelasticity on vortex dynamics. In Fig. 4(a), we plotted the comparative results between Newtonian fluid and FENE-CR fluid at Wi=3. As shown in Fig. 4(a), St is slightly lower compared with Newtonian cases. As St is defined by the inverse of a vortex shedding period, the elasticity attenuates the vortex shedding frequency. This trend is consistent with stationary cylinder case (Oliveira, 1999). In Fig. 4(a), the gap of St values between Newtonian and viscoelastic fluid becomes smaller with increasing α at $\alpha \le 1.5$. Vortex shedding at Wi=3 eventually disappears for $\alpha > 1.6$, which is smaller than the Newtonian case ($\alpha = 1.8$). Thus, it is obvious that the elasticity contributes to more suppress the vortex shedding in the flow past a rotating cylinder compared to the Newtonian case. We also investigated the fluctuations of amplitudes (Fig. 4(b)) and the mean values of drag and lift coefficients (Figs. 4(c) and 4(d)). As shown in Fig. 4(c)-(d), $C_{D(avg)}$ and $C_{L(avg)}$ of FENE-CR fluid at Wi=3 are not so much different from Newtonian case in the range of $0 \le \alpha \le 1.5$: the differences in $C_{D(avg)}$ and $C_{L(avg)}$ between FENE-CR fluid at Wi=3 and Newtonian fluid are less than 10%. However, as shown in Fig. 4(b), the magnitudes of fluctuations of FENE-CR at Wi=3 are much different from the Newtonian cases. Fig. 4(b) represents the limiting loop of C_L vs. C_D: the lines are constructed by connecting points of (C_D, C_L) in oscillatory vortex shedding for FENE-CR and Newtonian fluids. In

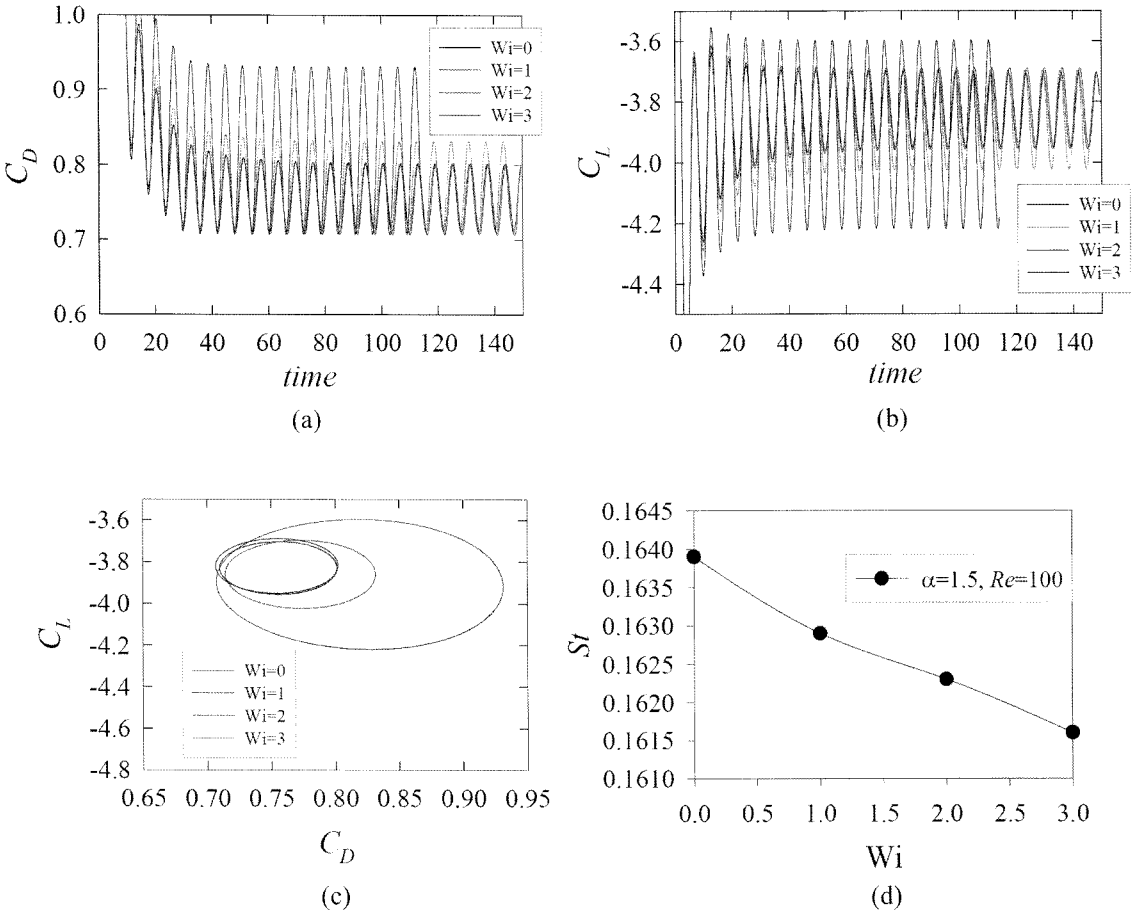

Fig. 5. Viscoelastic effect on the vortex shedding dynamics: (a) C_D vs time, (b) C_L vs time, (c) C_L vs C_D, and (d) St vs Wi at Re=100 and α=1.5.

the present work, the polymer contribution is not significant, *i.e.*, $\eta_p/\eta_0=0.1/1.1$. However, it significantly reduces the fluctuation of vortex shedding, which means that even small amount of polymer addition can contribute to dramatic change in the dynamics of vortex shedding at least under the present conditions considered, though the small amount of polymer contribution does not affect so much the mean values of drag and lift coefficients. We present the change of the oscillatory behaviors with increasing Wi at Re=100 and α=1.5 in Fig. 5. We considered Re=100 and α=1.5 case since the vortex shedding disappears for α>1.5 at Wi=3. As shown in Figs. 5(a)-(c), the fluctuations become reduced with increasing Wi. However, the trend is predicted to be saturated for Wi>2. As shown in Fig. 5(d), St slightly decreases with increasing Wi.

In Figs. 6(a)-(b), we show the variation of drag and lift coefficients vs. time with increasing Wi at Re=100 and α=5, in which condition the secondary vortex mode was predicted for Newtonian fluid by Stojković *et al.* (2003). Our simulation also predicts that the vortex shedding is obviously generated. In Figs. 6(a)-(b), two periods of waves are presented and the waves are very irregular, which is also observed by Stojković *et al.* (2003). *St* of the present work is predicted to be 0.023 for Newtonian fluid, which is in good agreement with the value ($\approx$0.022) obtained by Stojković *et al.* (2003). As shown in Figs. 6(a)-(d), the elasticity dramatically changes vortex dynamics and the vortex shedding completely disappears at Wi=2. However, the variation of St is complicated with increasing Wi as shown in Fig. 6(c). As shown in Figs. 6(a)-(b), the periods in C_D and C_L increase at low values of Wi (near Wi=0.25) and decrease again with more increasing Wi. As shown in Fig. 6(d), the fluctuations of C_D and C_L are dramatically reduced with increasing Wi. The shape of limiting C_L vs. C_D curves changes from shell-like to egg-like shape, and the area reduces with increasing Wi, which means the stabilizing effect of viscoelasticity. In Fig. 7, the flow patterns of Newtonian fluid around a rotating cylinder (α=5) are presented for one period at Re=100. In the figure, we observe that there is a circulating flow zone around the cylinder, of which the shape is similar to an egg. In each cycle, the egg-like flow zone grows in size (Figs. 7(a)-(b)) and pertains for a long time (Figs. 7(c)-(h)). Then, the egg-like flow zone collapses onto the cylinder (Figs. 7(i)-(j)) and it repeats the cycle. This cycle was also previously observed by by Stojković *et al.* (2002). In Fig. 8,

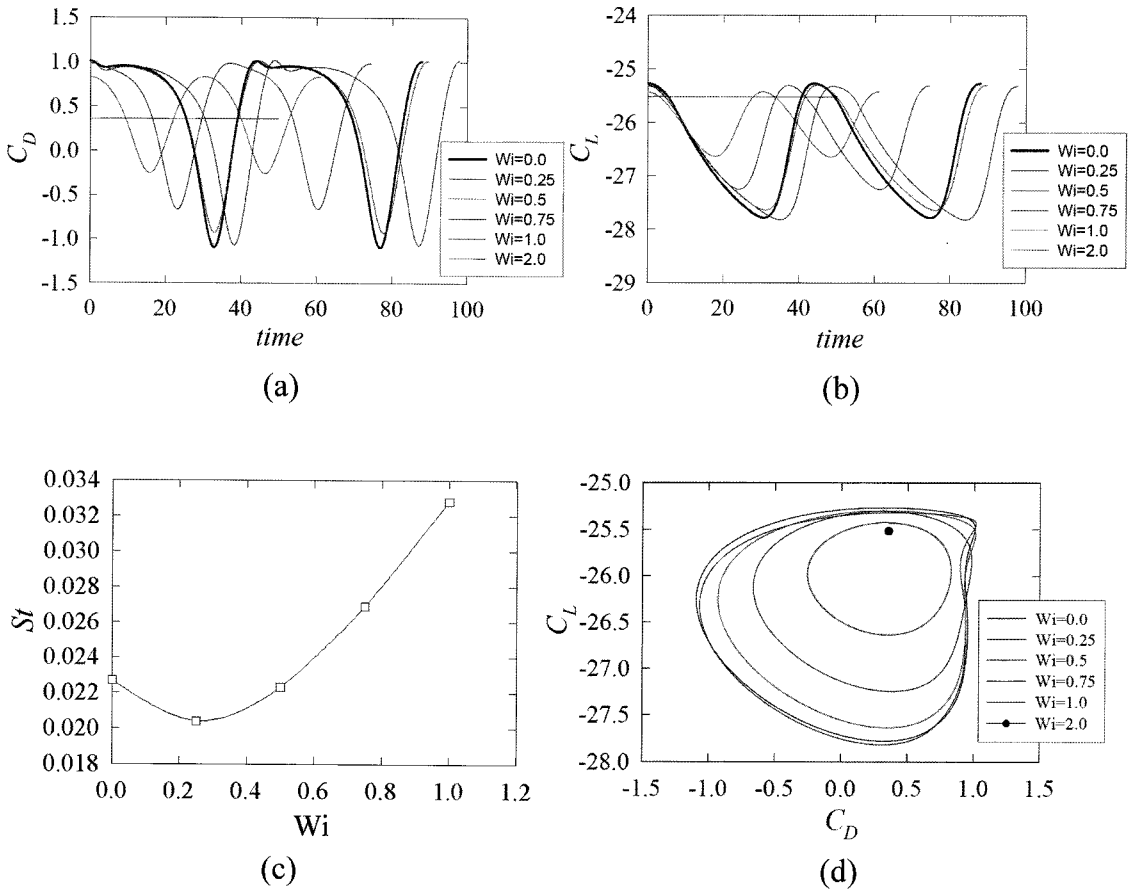

Fig. 6. Viscoelastic effect on the secondary-mode vortex: (a) C_D vs time, (b) C_L vs time, (c) C_L vs C_D, and (d) St vs Wi at Re=100 and α=5.

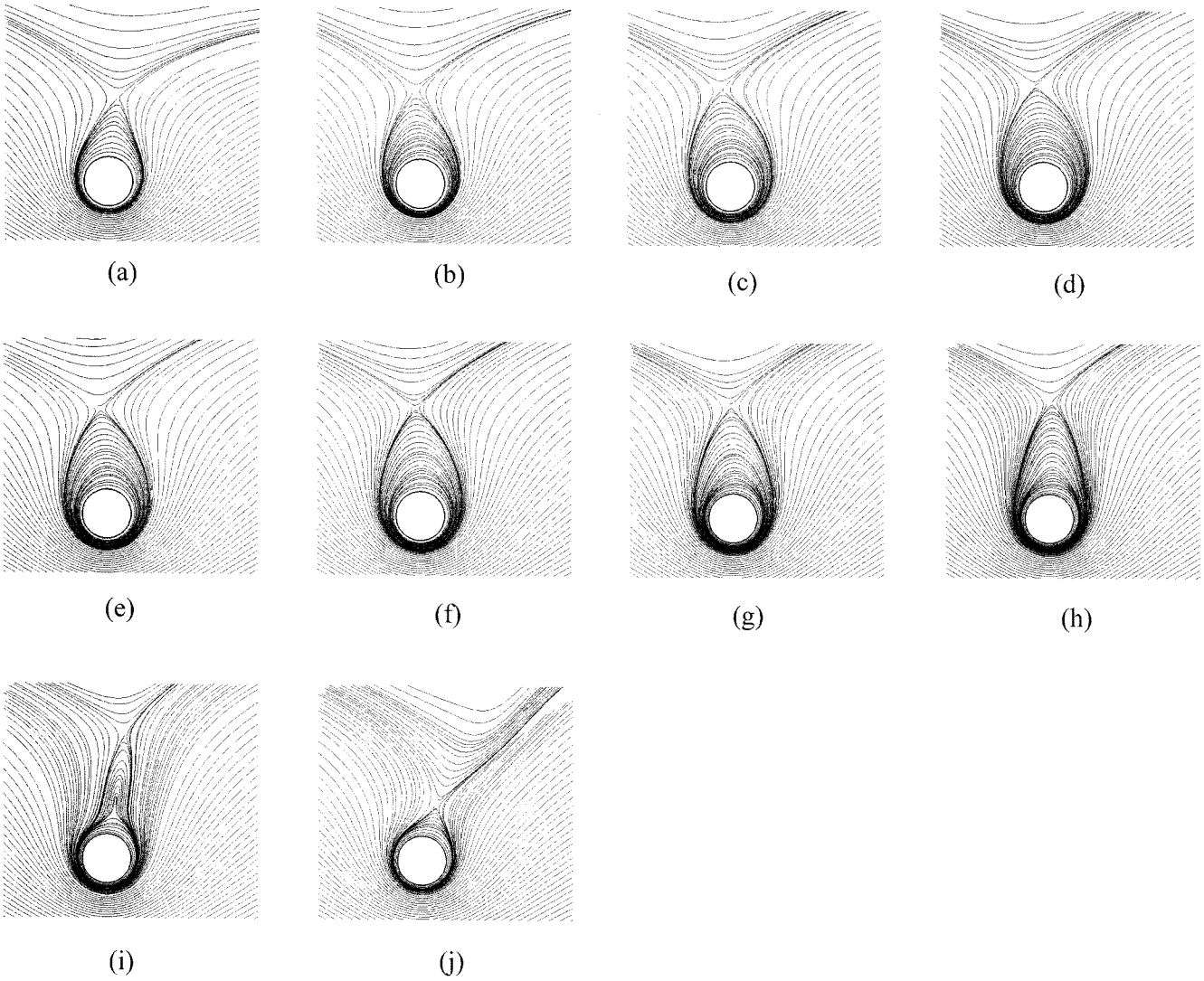

Fig. 7. Instantaneous streamlines around the cylinder for Newtonian fluid at Re=100, α=5: t/T=a) 1/10, b) 2/10, c) 3/10, d) 4/10, e) 5/10, f) 6/10, g) 7/10, h) 8/10, i) 9/10, j) 1, where T denotes the period of vortex shedding.

we present the stabilized flow field of viscoelastic fluid (Wi=2) at Re=100 and α=5. We observe the steady circulating flow zone around the cylinder of which the shape is also egg-like.

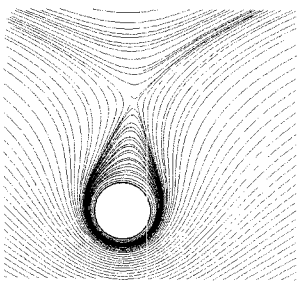

Fig. 8. Streamlines around the cylinder for viscoelastic fluid at Re=100, α=5 and Wi=2.0.

5. Conclusions

In this work, we employed a fully implicit transient numerical algorithm based on FEM with an iterative solution method and OBC method. We investigated the influence of elasticity on the vortex shedding in the flow past a rotating cylinder with FENE-CR model. According to the observation of the present study, we can conclude as follows:

(1) For $0 \leq \alpha \leq 2$, the frequency is slightly attenuated with increasing Wi numbers. The difference in St values between Newtonian and FENE-CR fluids becomes reduced with increasing α up to α=1.5. The fluctuations of C_D and C_L are dramatically reduced for FENE-CR fluid. The vortex shedding disappears at smaller α in the case of Wi=3: the critical α is 1.6, whereas the critical α is 1.8 for Newtonian fluid.

(2) At α=5, we observe that the secondary vortex mode occurs for Newtonian fluid. In this regime, the viscoelasticity dramatically affects the dynamics of vortex shedding. The vortex shedding disappears at Wi=2. The variation of St number is not monotonic with increasing Wi. Instead, St has a minimum near Wi=0.25.

The present study clearly shows that the viscoelastic effect significantly contributes to suppress the vortex shedding in flows around a rotating cylinder. We expect that this study will be helpful for future experimental design and provide a useful strategy to stabilize vortex shedding.

Acknowledgements

This study was also supported by research grants from the Korea Science and Engineering Foundation (KOSEF) through the Applied Rheology Center (ARC), an official KOSEF-created engineering research center (ERC) at Korea University, Seoul, Korea. This work was also supported by New Faculty Grant provided by Ajou University in 2008. The authors acknowledge the support from KISTI (Korea Institute of Science and Technology Information). The use of the computing system of the Supercomputing Center is also greatly appreciated. The authors also thank to Prof. Sangmo Kang in Dong-A University for providing us with data presented in Fig. 3.

References

Alves, M. A., F. T. Pinho and P. J. Oliveira, 2001, The flow of viscoelastic fluids past a cylinder: finite-volume high-resolution methods, *J. Non-Newtonian Fluid Mech.* **97**, 207-232.

Brooks, A. N. and T. J. R. Hughes, 1982, Streamline upwind/Petrov-Galerkin formulations for convection dominated flows with particular emphasis on the incompressible Navier-Stokes equations, *Comput. Mrthods Appl. Mech. Eng.* **32**, 199-259.

Cadot, O. and M. Lebey, 1999, *Phys. Fluids* **11**, 494-496.

Cadot, O. and S. Kumar, 2000, *J. Fluid Mech.* **416**, 151-172.

Caola A. E., Y. L. Joo, R. C. Armstrong and R. A. Brown, 2001, Highly parallel time integration of viscoelastic flows, *J. Non-Newtonian Fluid Mech.* **100**, 191-216.

Carew, E. O. A., P. Townsend and M. F. Webster, 1993, A taylor-petrov-galerkin algorithm for viscoelastic flow, *J. Non-Newtonian Fluid Mech.* **50**, 253-287.

Deville, M. O., P. F. Fischer and E. H. Mund, 2002, High-order methods for incompressible fluid flow, Cambridge University Press, Cambridge, UK.

Dimitropoulos, C. D., R. Sureshkumar and A. N. Beris, 1998, Direct numerical simulation of viscoelastic turbulent channel flow exhibiting drag reduction: effect of the variation of rheological parameters, *J. Non-Newtonian Fluid Mech.* **79**, 433.

Fan, Y. and M. J. Crochet, 1995, High-order finite element methods for steady viscoelastic flows, *J. Non-Newtonian Fluid Mech.* **57**, 283-311.

Graham, M. D., 2003, Interfacial hoop stress and instability of viscoelastic free surface flows, *Physics Fluids* **15**, 1702-1710.

Groisman, A. and V. Steinberg, 2000, Elastic turbulence in a polymer solution flow, *Nature* **405**, 53-55.

Kang, S., H. Choi and S. Lee, 1999, Laminar flow past a rotating circular cylinder, *Phys. Fluids* **11**, 3312-3321.

Kang, S., 2006, Laminar flow over a steadily rotating circular cylinder under the influence of uniform shear, *Phys. Fluids* **18**, 047106.

Kim, J. M., C. Kim, K. H. Ahn and S. J. Lee, 2004, An efficient iterative solver and high-resolution computations of the Oldroyd-B fluid flow past a confined cylinder, *J. Non-Newtonian Fluid Mech.* **123(2-3)**, 161-173.

Lilek Z., S. Muzaferija, M. Perić and V. Seidl, 1997, Computation of unsteady flows using nonmatching blocks of structured grids, *Numer. Heat Transf. B* **32**, 403-418.

McKinley, G. H., R. C. Armstrong and R. A. Brown, 1993, The wake instability in viscoelastic flow past confined circular cylinders, *Phil. Trans. Roy. Soc. Lond. A* **344**, 265-304.

McKinley, G. H., P. Pakdel and A. Öztekin, 1996, Rheological and geometric scaling of purely elastic instabilities, *J. Non-Newtonian Fluid Mech.* **67**, 19-47.

Min, T., J. Y. Yoo and H. Choi, 2001, Effect of spatial discretization schemes on numerical solutions of viscoelastic fluid flows, *J. Non-Newtonian Fluid Mech.* **100**, 27-47.

Min, T., J. Y. Yoo and H. Choi, 2003, Maximum drag reduction in a turbulent channel flow by polymer additives, *J. Fluid Mech.* **492**, 91-100.

Nigen, S. and K. Walters, 2002, Viscoelastic contraction flows: comparison of axisymmetric and planar configurations, *J. Non-Newtonian Fluid Mech.* **102**, 343-359.

Oliveira, P. J., 2001, Method for time-dependent simulations of viscoelastic flows: vortex shedding behind cylinder, *J. Non-Newtonian Fluid Mech.* **101**, 113-137.

Oliveira, P. J. and A. I. P. Miranda, 2005, A numerical study of steady and unsteady viscoelastic flow past bounded cylinders, *J. Non-Newtonian Fluid Mech.* **127**, 51-66.

Papanastasiou, T. C., N. Malamataris and K. Ellwood, 1992, A new outflow boundary condition, *Int. J. Numer. Methods Fluids* **14**, 587-608.

Park, J., K. Kwon and H. Choi, 1998, Numerical solutions of flow past a circular cylinder at Reynolds number up to 160, *KSME Int. J.* **12**, 1200-1205.

Park, S. J. and S. J. Lee, 1999, On the use of the open boundary condition method in the numerical simulation of nonisothermal viscoelastic flow, J. *Non-Newtonian Fluid Mech.* **87(2-3)**, 197-214.

Rothstein, J. P. and G. H. McKinley, 1999, Extensional flow of a polystyrene Boger fluid through a 4:1:4 axisymmetric contraction/expansion, *J. Non-Newtonian Fluid Mech.* **86**, 61-88.

Sahin, M. and R. G. Owens, 2004, On the effects of viscoelasticity on two-dimensional vortex dynamics in the cylinder wake, *J. Non-Newtonian Fluid Mech.* **123**, 121-139.

Saramito, P. and J. M. Piau, 1994, Flow characteristics of viscoelastic fluids in an abrupt contraction by using numerical modeling, *J. Non-Newtonian Fluid Mech.* **52**, 263–288.

Spiegelberg H. and G. H. McKinley, 1996, Stress relaxation and

elastic decohesion of viscoelastic polymer solutions in extensional flow, J. *Non-Newtonian Fluid Mech.* **67**, 49-76.

Stojković, D., M. Breuer and F. Durst, 2002, Effect of high rotation rates on the laminar flow around a circular cylinder, *Phys. Fluids* **14(9)**, 3160-3178.

Stojković, D., P. Schon, M. Breuer and F. Durst, 2003, On the new vortex shedding mode past a rotating circular cylinder, *Phys. Fluids* **15(5)**, 1257-1260.

Sunwoo, G. B, S. J. Park, S. J. Lee, K. H. Ahn and S. J. Lee, 2001, Numerical simulation of three-dimensional viscoelastic flow using the open boundary condition method in coextrusion process, *J. Non-Newtonian Fluid Mech.* **99(2-3)**, 125-144.

Sureshkumar, R., A. N. Beris and R. A. Handler, 1997, Direct numerical simulation of the turbulent channel flow of a polymer solution, *Phys. Fluids* **9(3)**, 743-755.

Usui, H., T. Shibata and Y. Sano, 1980, *J. Chem. Eng. Jpn.* **13**, 77-79.

van der Vorst, H. A., 1992, Bi-CGSTAB: A fast and smoothly converging variant of Bi-CG for the solution of non-symmetric linear systems, *SIAM J. Sci. Stat. Comput.* **12**, 631-634.

Williamson, C. H. K., 1996, Vortex dynamics in the cylinder wake, *Annu. Rev. Fluid Mech.* **28**, 477-539.